Continuity and temperature dependence of the vortex-phase boundary of $Bi_2Sr_2CaCu_2O_{8+\delta}$

Y. Yamaguchi, G. Rajaram,* N. Shirakawa, A. Mumtaz,† H. Obara, T. Nakagawa, and H. Bando
Electrotechnical Laboratory, Tsukuba, Ibaraki 305-8568, Japan
(Received 15 February 2000; published 11 December 2000)

Local magnetization data of $Bi_2Sr_2CaCu_2O_{8+\delta}$ crystals measured using a Hall sensor array are reported for underdoped, optimally doped, and overdoped samples. Magnetization data just inside the sample edge provide the most reliable values for the vortex-phase transition field in the magnetic phase diagram among those at other positions. The first-order melting line (ML), which manifests itself as a step in magnetization $M(H)$, is detected at relatively high temperatures for all the samples. The position in the field of the second peak in magnetization at low temperatures can be determined unambiguously from the relaxed magnetization after a sufficiently long waiting time. It is found that in all the samples the onset field of the second peak, which is interpreted as an entanglement line (EL), connects continuously with ML as the temperature is increased. At intermediate temperatures, for the underdoped and optimally doped samples, either the second peak or the magnetization cusp, whose position connects with that of the step, is observed at the same temperature and the same field but in different experimental time scales. The ML for the three samples corresponds to a single curve when a scaling of $(T_C^2-T^2)/T_CT\lambda^2\gamma^2$ (T_C is the superconducting transition temperature, λ is the penetration depth, and γ is the anisotropy constant) is used against the induction B, consistent with the decoupling theory. The EL is well fitted by $B\propto(1+cT^2)/\gamma^2$, with $c>0$, suggesting a presence of dimensional crossover. The positions of the depinning line and the irreversibility line, measured by temperature sweep and field sweep, respectively, are found to depend on the time scale of the sweep rate, suggesting that they represent crossovers between two different vortex-creep mechanisms. Only the ML-EL is suggested to be the real phase boundary.

DOI: 10.1103/PhysRevB.63.014504 PACS number(s): 74.25.Dw, 74.25.Ha, 74.72.Hs

I. INTRODUCTION

Vortex-matter phase diagrams of high-T_C superconductors (HTSC) have been extensively investigated as a new stage of physics as well as from the technological point of view.[1] Among various HTSC, the $Bi_2Sr_2CaCu_2O_{8+\delta}$ (Bi2212) system attracts special attention, because it is a typical layered system playing a crucial role in the physics of HTSC. When the external field is applied in a direction normal to the layer (plane), vortices are confined within the superconducting CuO_2 bilayers like ''pancakes'' and couple through Josephson and electromagnetic interaction between adjacent layers. The pancakes form vortex lines at low temperature and in low field, and form a vortex lattice. With increasing temperature the lattice melts into a fluid resulting in a magnetization step[2–4] as in a first-order phase transition. This first-order phase transition forms a melting line (ML) that has been reported to terminate at a critical point at some intermediate temperature in the H-T plane.[4] Recently, Fuchs *et al.*[5] have proposed a rather complicated phase diagram that includes an irreversibility line (IL), a depinning line (DL), and a second-peak field with the suggestion that these lines connect with the ML at the critical point. As far as the second peak in magnetization is concerned, it has been suggested that it is the onset field of the second peak that is relevant to the phase diagram, forming a vortex-entanglement line (EL), a disorder-driven transition,[6–8] above which field the second-peak in magnetization appears. A phase diagram that includes some entanglement phases has been proposed by other workers also, via experiment.[9] The Bi2212 system has in it a disordered system of weak point pinning centers due to oxygen defects. The situation at present is that, while it has been verified[10,11] that the vortices in low fields form a vortex lattice (or Bragg lattice) below the EL and ML, in high fields above the EL, vortices are very glassy and features such as the second magnetization peak and IL exhibit pronounced dependence on relaxation effects.[2,12,13] In addition, these phase boundaries are expected to shift depending on the pinning character controlled by the oxygen concentration.[14,15] The continuity between these phase boundaries, their analytical form as well as the dependence of these features on oxygen doping, need to be clarified more definitively. It has been generally accepted that a measurement of the local magnetization is crucial for the study of the phase boundaries.[4,12,16] In this paper we report an investigation of the phase boundaries of underdoped, optimally doped, and overdoped Bi2212 crystals, in which measurements have been made using a micro-Hall sensor array to take into account the spatial profiles of magnetization across samples and the effects of the magnetic relaxation. The study yielded interesting results particularly in the intermediate temperature region of the phase diagram, where either the second magnetization peak or the magnetization cusp, whose position in the phase diagram connects with that of the step, could be observed, depending on the time scale of the measurement.

II. SAMPLE AND MEASUREMENT

The single crystals of Bi2212 were grown by the traveling-solvent floating-zone method using an infrared-radiation furnace. The samples were cut into small pieces

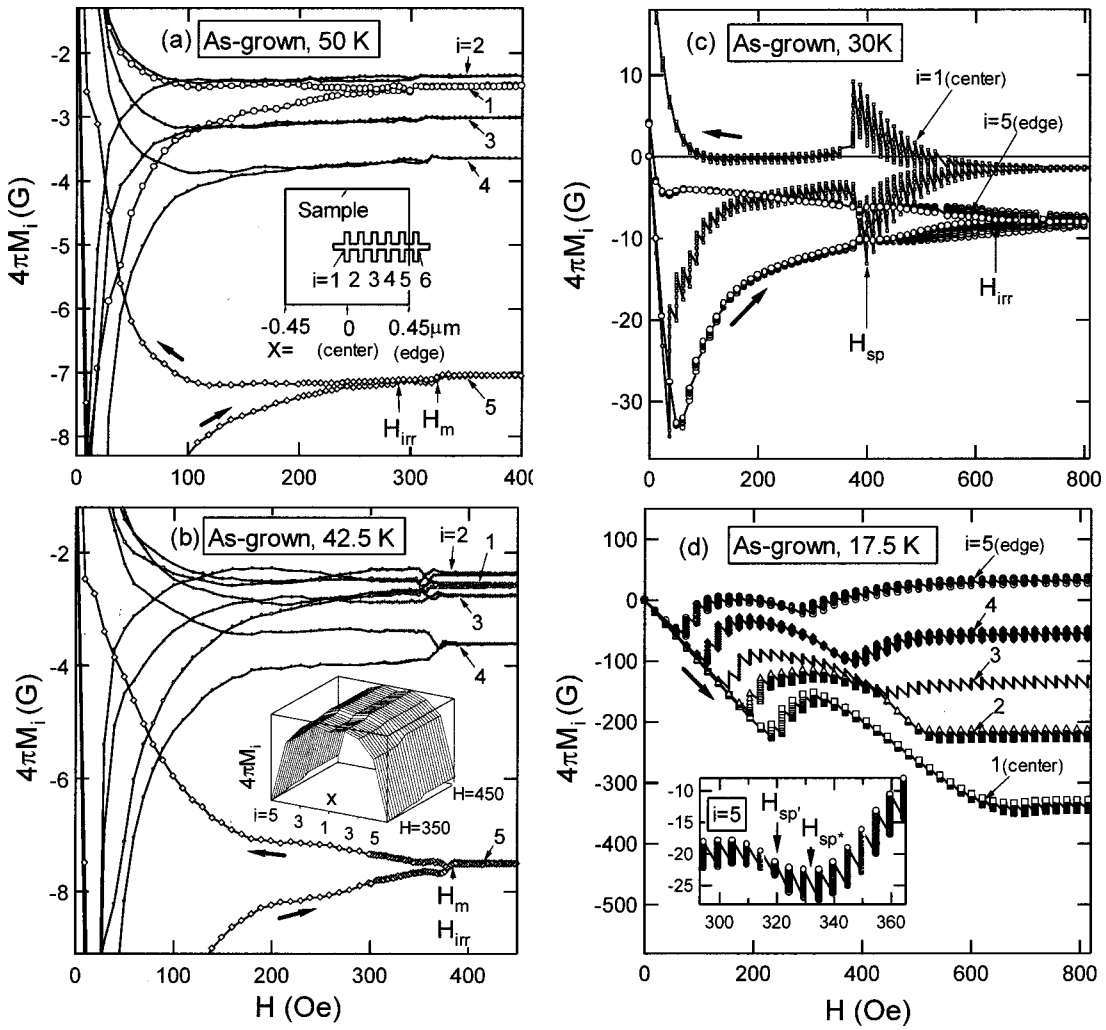

FIG. 1. Magnetization curves ($4\pi M_i$ vs H) at (a) 50 K, (b) 42.5 K, (c) 30 K, and (d) 17.5 K, where $i=1-5$ is the sensor number as shown in the inset of (a). The thick arrows indicate the direction of the field sweep. To elicit time evolution of M_i, data with various pause times at each field are shown: (a) and (b) 150 s, (c) 20–300 s, (d) 20–600 s; inset of (d) 20 s to 3 h. H_m is the melting field, $H_{\rm irr}$ the irreversibility field, and $H_{\rm sp}$ the second peak field. Inset of (b) shows spatial profile across the sample near H_m.

with a typical dimension of $0.9\times0.8\times0.03\,\mathrm{mm}^3$, with the crystal c axis perpendicular to the plate. A sample, named #*A*, was an as-grown crystal with a composition of $Bi_{2.1}Sr_{1.9}CaCu_2O_{8+\delta}$, and determined to be an almost optimally doped one.[15] A considerably overdoped sample (#*O*) was a $Bi_{2.1}Sr_{1.9}CaCu_2O_{8+\delta}$ crystal annealed at 380 °C in a pure-oxygen atmosphere for a week. A third sample, #*U*, was an underdoped one with composition $Bi_{2.2}Sr_{1.8}CaCu_2O_{8+\delta}$, prepared by annealing at 730 °C in air for a day and quenching subsequently in liquid nitrogen. The superconducting transition temperature T_C was 71.5, 90.5, and 80.5 K for samples #*O*, #*A*, and #*U*, respectively.[15] The Hall sensor array was fabricated from a $GaAs/Al_xGa_{1-x}As$ multilayer film with two-dimensional (2D) electron gas as the active layer. The array consisted of seven sensors each with active area $15\times15\,\mu\mathrm{m}^2$. Six sensors, used to measure magnetic induction B_i $(i=1-6)$ at the sample surface, were separated by 0.1 mm from each other, and one sensor, used to measure external field H, was separated by 2.5 mm from the others. The external field H was produced by a superconducting solenoid and was applied parallel to the crystal c axis. The magnetic induction B_i and field H were determined by measuring the Hall voltages using four two-channel dc voltmeters simultaneously. Spatial profiles measured on the overdoped sample #*O* have been reported elsewhere.[16]

III. EXPERIMENTAL RESULTS

A. Spatial profile of magnetization and the characteristic fields

Spatial profiles, across the sample, of magnetization ($4\pi M_i$ vs H curves, where $4\pi M_i=B_i-H$, with $i=1-5$), are shown for the as-grown (almost optimally doped) crystal in Figs. 1(a)–1(d). In order to elicit the time evolution (relaxation) at each field, data at some temperatures were taken by sweeping the external field H by a ramp-and-pause method, with a pausing time t_p divided into several acquisition times (~20 s). The data in Figs. 1(c) and 1(d) show results of such a measurement. Above 50 K, as shown in Fig. 1(a), a distinct magnetization step, attributable to the first-order phase transition, was observed at field H_m, while the

spatial magnetization profile measured by sensors 1–5 was dome shaped ($|M_1|>|M_5|$), as shown in the inset of Fig. 1(b). With decreasing temperature, the magnetization step was deformed due to magnetic hysteresis [Fig. 1(b)]. At 30 K [Fig. 1(c)] the magnetization profile deviated from the dome shape near the field H_{sp} ($\sim$390 Oe), where the second peak appeared.

The envelopes of data at various acquisition stages during the pausing time corresponded to magnetization curves with various relaxing times. It was observed that the second peak diminished rapidly with increasing relaxation time. At 17.5 K [Fig. 1(d)] the profile became V shaped ($|M_1|>|M_5|$) at almost all fields measured. The second peak became larger and broader with decreasing temperature [note the scales in Fig. 1(d)].

The irreversibility field H_{irr}, where the magnetic hysteresis vanished, was sensitive to the criterion used to define ''irreversibility'' and the measurement time, as shown in Fig. 1(c). In the present work, the criterion for vanishing hysteresis was, in accordance with experimental errors, 0.02 G in low field and 0.1 G in high field. Near 50 K, H_{irr} was observed to be below H_m, i.e., in the solid phase, and approached H_m with decreasing temperature. At 42.5 K [Fig. 1(b)], H_{irr} almost coincided with H_m, and the magnetization step was reversible for part of the transition. At 30 K [Fig. 1(c)], H_{irr} well exceeded the position H_{sp} of the second peak, which appeared abruptly for lower temperatures instead of the magnetization step. The H_{irr} ($\sim$630 Oe) in Fig. 1(c) was based on data for $t_p=2$ min, while it shifted to $\sim$420 Oe for a longer relaxation time $t_p=2$ h.

The second peak field H_{sp} was found to depend on the position i, but was, however, almost independent of B. Among the various sensors, the data acquired by the sensor $i=5$ positioned just inside the sample edge needed the least corrections for the internal induction and are used for further analysis. Also, the peak was observed most clearly in this position. In order to determine values of H_{sp}, we examined the field $H_{sp'}$ where $|dM/dH|$ was maximum, and the field H_{sp*}, where M itself had the peak value. In the present study, it was found that H_{sp*} decreased when the magnetization was allowed to relax for longer times while $H_{sp'}$ increased only slightly. In other words, the second peak of $M(H)$ itself evolved sharply on the low-field side when allowed to relax for sufficiently long periods. Therefore, $H_{sp}=(H_{sp*}+H_{sp'})/2$ was taken to be extrapolated value for the position of the second peak in the limit of infinitely long relaxation times, with an experimental error $H_{sp*}-H_{sp'}$. In the inset of Fig. 1(d), the value B_{sp} ($=H_{sp}+4\pi M_{eq}$) was evaluated to be 319 G, with $H_{sp*}=334$ G, $H_{sp'}=320$ G, and $4\pi M_{eq}=-8$ G. The second peak was observed even at 15 K at the sample center, but was obscured by the first peak near the sample edge. The second peak was observed down to 15 K and to 12.5 K, respectively, for the underdoped and overdoped sample.

B. Change from the magnetization step to the second peak

In this section the magnetization step and the second peak at the $i=5$ sensor (near the sample edge) are described. Figure 2 shows temperature dependence of the *M-H* curves having the magnetization step and the second peak for the as-grown, the underdoped, and the overdoped samples, respectively. In Figs. 2(a), 2(c), and 2(e), the data correspond to those at the end of the pause time t_p at each measured field. These figures illustrate the crossover from a *complete* magnetization step in the sense that $M(H)$ is fully reversible during the transition with $H_{irr}<H_m$ to an *incomplete* one, in which $M(H)$ is reversible for part of the transition with $H_{irr}\sim H_m$. Figures 2(b), 2(d), and 2(f) show the time evolution in the magnetization curves and illustrate the detailed changes from the step to the peak.

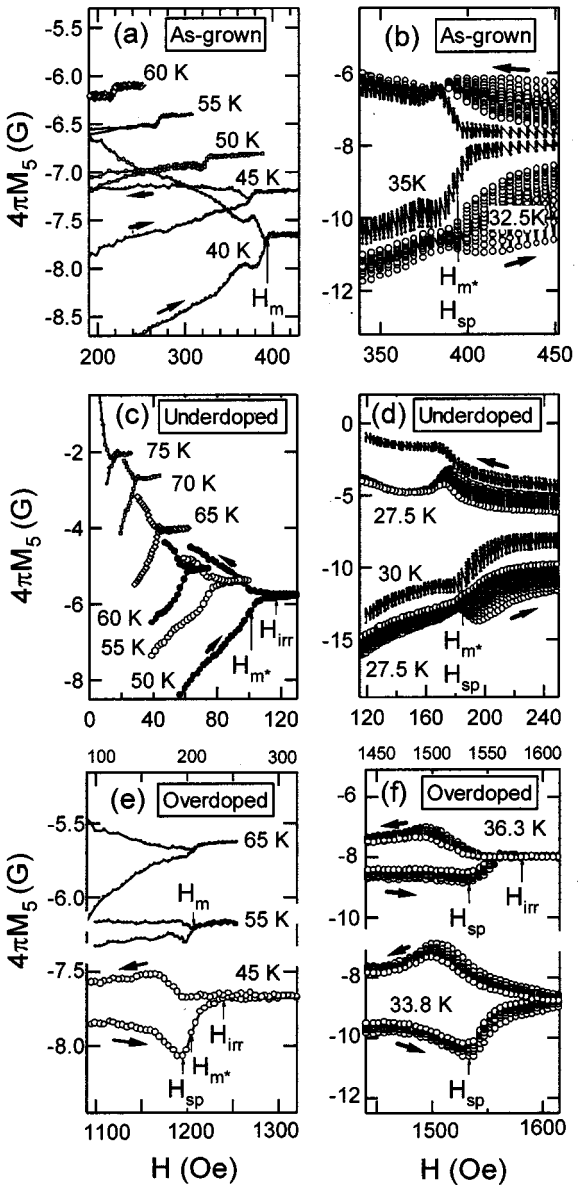

FIG. 2. Temperature-driven crossover from the first-order transition to the second peak in the magnetization curves. (a) and (b) for the as-grown sample; (c) and (d) for the underdoped sample; and (e) and (f) for the overdoped sample. The data are for the sensor $i=5$ (near the edge). (a), (c), and (e) show the data after an evolved time of 150 s at each field; in (b), (d), and (f) evolved time is between 20 and 300 s.

For the as-grown sample [Figs. 2(a) and 2(b)], a *complete* magnetization step was observed above 50 K. The step was *incomplete* in the temperature interval 45 to 40 K. At 35 K a reversible magnetization step was not observed in *M-H* curves, but a sharp cusplike peak was observed. The position of this cusp, as defined by the field H_{m*} where the maximum in dM/dH occurs in the ascending field, was at a field smaller than $H_{\rm irr}$. At 32.5 K, a second peak at $H_{\rm sp'}$ was observed when a fast ramp rate of the applied field was used, while a cusp was observed at H_{m*} when a slow ramp rate was used. This evolution from the second peak to the cusp is more clearly demonstrated in Fig. 5(b), where data at different acquisition stages of the ramp-and-pause method are shown. The value $H_{\rm sp'}$ for the onset field of the second peak agrees with the value H_{m*} for the cusp. This enables us to switch the characteristic fields smoothly from the H_{m*} (a maximum in dM/dH) for the cusp to the $H_{\rm sp'}$ (a minimum in dM/dH) for the second peak. It was observed that the error, $H_{\rm sp'}-H_{m*}$, in the position of the second peak nearly vanished at 32.5 K. Since the value H_{m*} for the cusp connects smoothly with the melting field H_m, the second peak line (denoted EL here) in the phase diagram connects smoothly with the ML independent of the definition of the position of the second peak.

This time-dependent crossover from the peak to the cusp was also observed for the underdoped sample at 27.5 K, as shown in Fig. 2(d). For this sample, the magnetization step was observed in a rather restricted temperature region above 70 K close to T_C (=80.5 K). The sharp change in magnetization at H_{m*} was observed between 65 and 30 K, a wider range of temperatures than the case of the optimally doped sample. In contrast, for the overdoped sample [Figs. 2(e) and 2(f)], the time-dependent crossover was not clearly observed. The second peak or the cusp in the *M-H* curve was observed in the temperature interval 35–45 K, with the second peak gradually evolving into a cusp with increasing temperature.

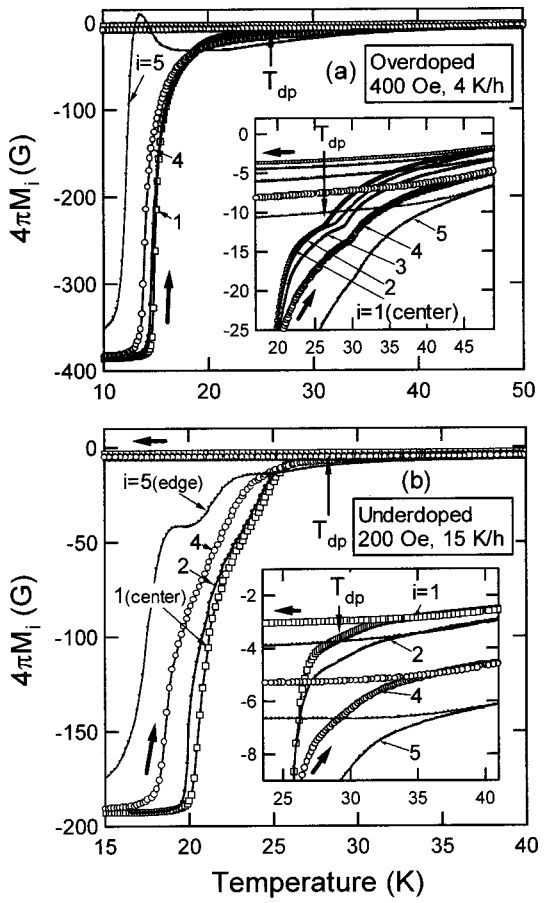

FIG. 3. Temperature dependence ($4\pi M_i$ vs T, with $i=1-5$) of the zero-field-cooled (warm-up branches) and the field-cooled (cool-down branches) magnetization for (a) the overdoped sample and (b) the underdoped sample. Thin arrows show the depinning temperature $T_{\rm dp}$ for $i=1$, (sample center). The insets are expanded views near $T_{\rm dp}$.

C. Depinning line and phase diagram

Another characteristic temperature, the depinning temperature $T_{\rm dp}$ (denoted as T_{d1} and T_{d2} by Dewhurst and Doyle[17]) was examined by sweeping temperature at constant field. The magnetization on warming up after cooling the sample in the zero field is indicative of the characteristic process temperatures by which the external field enters into the sample. Figure 3(a) shows the $4\pi M_i$ vs T ($i=1-5$) curves at $H=400$ Oe for the overdoped sample. After cooling the sample in the zero-field, the external field was applied at 10 K. With increasing temperature, the field entered rapidly into the sample above ~14 K. The spatial profile of magnetization was V shaped at low temperatures, then changed into a dome-shaped one and gradually became flat near T_C. In this process, a distinct kink in the $4\pi M_i$ vs T curves was observed at $T_{\rm dp}\sim 26$ K at the sample center and at 31 K near the sample edge. When the temperature sweep rate was changed from 4 to 60 K/h, these kink positions $T_{\rm dp}$ increased by ~2 K. The kink was observed for all the measured field below 1400 Oe when the local magnetization $4\pi M$ became nearly −10 G. This kink was observed for the as-grown sample also at nearly the same temperature (~28 K), where in this case also magnetization was nearly −10 G. For the underdoped sample, the kink below the melting line was scarcely observed. However, a weak trace of the kink was barely observed at a high field above the melting line, as shown in Fig. 3(b). For the overdoped sample and the as-grown one, the kink or shoulder at high field (T_{d1} in Ref. 17) was not observed.

Figure 4 shows the phase diagram including all the observed characteristic fields and the temperatures. We show the phase diagram in the *B-T* plane, where the local induction B is smaller than the applied field H by about 8 G ($=4\pi M_{\rm eq}$ at the edge sensor), which goes to zero at T_C. The crossover from the second peak to the cusp is indicated by superposing some symbols on $B_{\rm sp}$ and B_{m*}. The crossover for the as-grown and the underdoped sample took place at the top of the hump formed by these two characteristic fields. For these samples, the critical temperature $T_{\rm cr}$ was defined as the highest temperature where the second peak was observed. The $T_{\rm cr}$ was 32.5 and 27.5 K for the as-grown

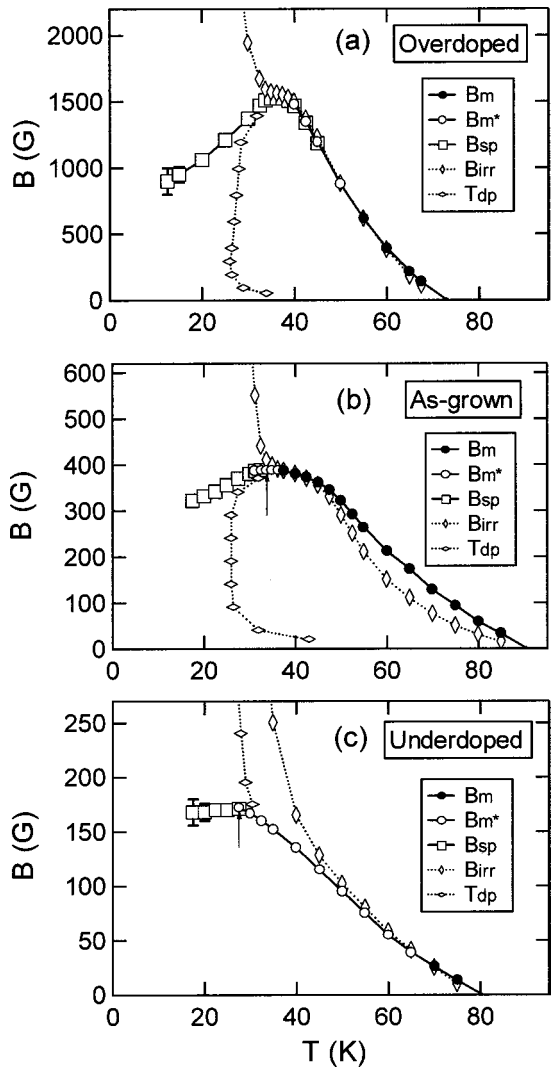

FIG. 4. Phase diagrams of the overdoped (a), the as-grown (b), and the underdoped sample (c). The B_m for the melting transition and the position B_{m*} of the cusp in magnetization. The error bar for B_{sp} is explained in the text. Arrows indicate the critical point.

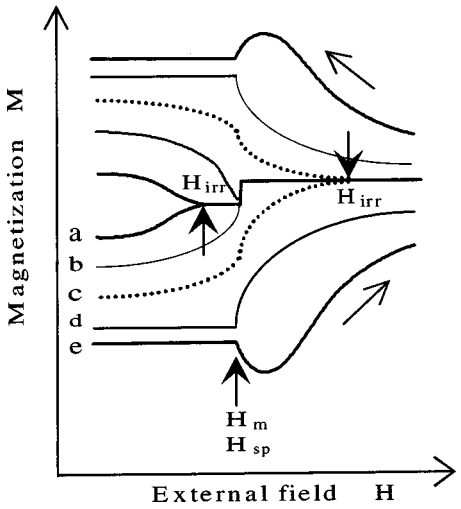

FIG. 5. Evolution of the $4\pi M$ vs H curves with decreasing temperature: traces from *a* to *e* demonstrate the crossover between the magnetization step of the vortex-lattice melting at H_m and the second peak at H_{sp}. Long arrows show direction of field sweep. The H_{irr} shows the irreversibility field below and above H_m.

and the underdoped sample, respectively. For all the samples, the DL for $T_{dp}(B)$ seemed to terminate at the T_{cr}. All the IL for $B_{irr}(T)$ connected smoothly with the ML.

IV. DISCUSSION

A. Continuity of the phase boundary

The evolution of the magnetization step to the second peak as the temperature is decreased occurs for all the samples and has the common features depicted schematically in Fig. 5. Curve *a* shows a *completely reversible* magnetization step with $H_{irr}<H_m$, and curve *b* shows a step with the irreversibility setting in at H_m, i.e., $H_{irr}\sim H_m$. Curves *c* and *d* show sharp change or cusps in magnetization, which suggests an abrupt softening of the vortex solid at H_{m*}, the position of the steplike peak of the cusp, with $H_{irr}>H_{m*}$. We emphasize that the $H_{m*}(T)$ line is well defined and connects smoothly with the second peak line at low temperatures and to the melting line at high temperatures. H_{m*} thus appears to be a *remnant* of the magnetization step for the first-order phase transition at the temperature region higher than the ''critical point,'' and extends into the temperature region lower than the critical point. Finally, curve *e* shows the second peak, which exhibits a kink at $H_{sp'}$. All the curves in Fig. 2 have a tendency to follow this sequence with decreasing temperatures. The second peak appears to evolve into a cusp (curve *c*) if magnetization is relaxed for sufficiently long times. This time evolution plays a key role in demonstrating the clear continuity between the step and the second peak in magnetization.

The evolution of the second peak to a cusp with relaxation described above is not quite well defined in the overdoped sample. Both the second peak and the cusp are sharp at intermediate temperature, and there is a broadening below H_{m*} with a sharp cutoff at H_{m*} at high temperatures. This broadening is not observed in the underdoped sample and is probably caused by an increase of the pinning strength due to excess oxygen. This explanation is similar to that given by Ooi *et al.*,[18] who have also suggested that H_{m*} is a remnant of the first-order phase transition. In the underdoped sample, the temperature range over which the magnetization step is detected is considerably limited relative to the as-grown sample, and the intermediate temperature region over which the cusp occurs at large relaxation times is extended. One probable reason for this could be inhomogeneity in the sample, which is suggested from the transition width of ~2.5 K compared with ~0.3 K for the overdoped sample.[15] Another reason may be the surface/geometrical barrier, which contribute to large hysteresis at low fields[19] and which are incompletely suppressed at H_{m*}. The irreversibility field H_{irr} is thus much larger than H_{m*}. The observed $B_{m*}(T)$ line for the underdoped sample as well as for the overdoped

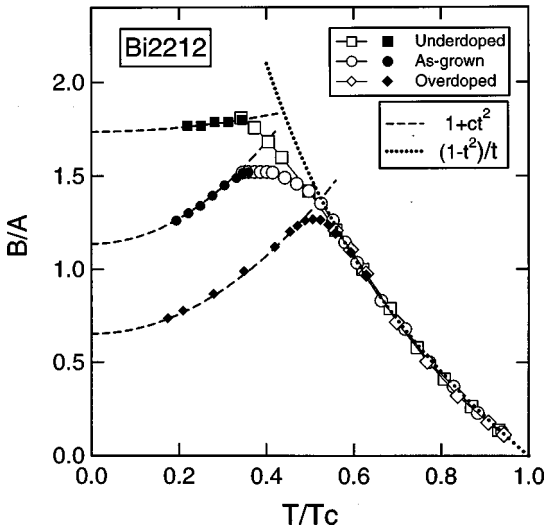

FIG. 6. A unified phase diagram for three samples. Open symbols correspond to B_{m*} (cusp) and B_m (step) to make up the melting line (ML), while the filled symbols correspond to the B_{sp} (entanglement line). *A* is the value used to normalize the *B* axis to fit a curve $(1-t^2)/t$ for ML. The best fit parameters are summarized in Table I.

one is *remnant* of the $B_m(T)$ line, i.e., the ML. The $B_m(T)$ line that connects directly to the EL is probably realized only for the optimally doped *ideal* sample, of which the as-grown sample in the present study is a close representative. However, it is difficult to decide whether EL is the first- or second-order boundary from the present measurement, because it is not clear that the second peak changes into a step even after a long relaxation time.

The melting line is expected to be independent of the sample position at which it is determined after correcting for the induction profile arising from various pinning mechanisms. However, the difference between the melting field H_m [e.g., ~320 Oe in Fig. 1(a)] near the sample edge ($i=5$ sensor) and that at the center (~ 300 Oe) ($i=1$ sensor) was larger than the difference (~8 Oe due to the dome-shaped profile) in *B*. A probable reason for this difference may be a stray field in an unavoidable gap between the sample surface and the active layer of the Hall sensor. A positive shift in magnetization, M_5, near the sample edge in high field at 17.5 K [Fig. 1(d)] may also be due to this stray field, which becomes larger with increasing internal induction to be excluded. Broadening of the second peak at the sample center may be the result of superposition of various relaxation effects arising from varying distances from the sample edge in a square shape. Due to these effects systematic errors of a few percent ($\sim 12/320 \sim \Delta H/H_m$) on the field axis are expected.

B. Temperature dependence of the phase boundary

The ML-EL curves of the phase diagram in Fig. 4 for all the three samples are replotted in Fig. 6, where the temperature axis is now the reduced temperature $t=T/T_C$. Then all the ML, except in a narrow intermediate temperature region, can be fitted by a dependence $A(1-t^2)/t$, as in previous reports.[4,15] This fit is better than others such as $(1-t)^n$, $(1-t)^n/t$, or $(1-t^2)^n/t$ for $n>1$.[20] It is noted that the $(1-t^2)/t$ dependence is expected for the decoupling transition,[21,22] while a $(1-t^2)^{1.5}/t$ dependence is predicted by the melting theory.[23] Here, $\lambda^2=\lambda_0^2/(1-t^2)$ has been used for the temperature dependence of the penetration depth λ instead of $\lambda^2=\lambda_0^2/(1-t^4)$ from the two-fluid model, since we can better fit the observed[24] value of λ. On the low-temperature side, the EL curves are well fitted by an empirical dependence $B_0(1+ct^2)$, where B_0 is B_{sp} at $T=0$ obtained by extrapolation and c (>0) is a coefficient of the temperature-dependent part. The fitting parameters are summarized in Table I.

According to the decoupling theory,[20,22] the prefactor *A* should be given by

$$A=\alpha_D\Phi_0^3/16\pi^2 k_B T_C \lambda_0^2 \gamma^2 s, \tag{1}$$

where Φ_0 is the flux quantum, $\alpha_D \sim 0.1$ (Ref. 20) is a decoupling parameter, k_B is the Boltzman constant, λ_0 is the penetration depth at $T=0$, γ is the anisotropy constant, and *s* (~1.5 nm) is the distance between the adjacent CuO_2 bilayers. The observed value of *A* is successfully reproduced within the experimental errors with γ (Refs. 25 and 26) and λ_0,[27,28] as adjustable parameters given in Table I. This indicates that the decoupling scenario is favorable for explaining the ML. The decoupling feature has been suggested in a wide temperature region from mutual-inductance experiments[29,30] and more directly from the Josephson-plasma resonance measurement by Shibauchi *et al.*,[31] who found an abrupt decrease of the coherence parameter between pancake vortices at B_m.

Next, we try to explain observed temperature dependence of the EL, $B_{sp}=B_0(1+ct^2)$. The second peak at low temperature has generally been explained[12,14] as arising from the 3D–2D crossover.[32] When we use the γ values in Table I, the observed B_0 can be obtained with the expression

TABLE I. Observed values (T_C, *A*, B_0, and *c*) and the parameter (γ and λ_0) to fit *A* and B_0 for each sample.

Sample	T_C (K)	*A* (G)	B_0 (G)	*c*	γ	λ_0 (nm)
Overdoped	71.5	1225	800	4.0	107	164
As-grown	90.5	255	290	3.0	178	193
Underdoped	80.5	95	165	0.3	236	252

$$B_0 \sim \Phi_0 / \gamma^2 s^2 \tag{2}$$

of the 3D–2D crossover transition. However, this theory[32] does not include the temperature-dependent term ct^2. The temperature-dependent transition has been discussed in the context of entanglement theory[6,7] or the ''δl-pinning'' theory.[1] However, the entanglement theory[7] fails to predict the temperature dependence near $T=0$ for the highly anisotropic case; also it includes some parameters that are difficult to estimate such as a pinning energy (U_p) or a disorder parameter (Δ). On the other hand, the δl-pinning theory, which gives $B_{sp} \propto (1-t^2)^{-1/2}$, explains neither the large value of c nor the dependence of c on the oxygen stoichiometry. Another promising theory,[8] which involves generalizing the Lindemann criterion not only to the elastic energy but also to the pinning energy, predicts values close to Eq. (2) at $T=0$ and $B_{sp} \propto (1-t^2)^{-1}$ in some conditions, but it is cumbersome to estimate c. Therefore, all these theories are inadequate to explain the parameter c. In any case, it seems reasonable to speculate that c tends to zero in the limit of large γ, since c has a rather small value for the underdoped sample. We must postpone a more quantitative comparison with the theory until we have a more detailed theory and reliable estimates for the related parameters.

The continuity between the EL and ML is unambiguous because of the change of the second peak to a cusp with a sharp edge and peak at large relaxation times and from the cusp to the magnetization step with increasing temperature. The implication of this continuity is that the two phenomena (the second peak and the step) have a common underlying origin; the decoupling in the c axis as has been shown by an experiment.[31] It has been also shown[31] that some interlayer phase coherence (a few tens of percent) still persists above the decoupling field. However, at high temperature, the decoupling enables distortions of the vortex lines at point-pinning sites. At low temperatures, it is vortex decoupling between layers that triggers both a disorder-aided weakening of correlation of the vortex pancakes along the c axis at the EL and thermal fluctuation induced loss of correlation along the plane of weakly coupled vortex lines. The second peak becomes sharper and smaller, then comes to a cusp as the vortex segments relax into pinning sites with increasing relaxation times. This state is probably a weakly entangled state that has been proposed for a disordered system with strong point pinning.[6–8]

C. Crossover between the vortex-depinning characters

Finally, we discuss the depinning temperature T_{dp} and the irreversibility field B_{irr}. Until now, various characteristic phase boundaries in a solid phase below the ML-EL have been suggested to occur near 38–45 K from ac response[3,5] and near 20–32 K from static magnetization.[17,33] This variation is probably due to differences in the definition of the characteristics as well as relaxation effects. In the present work, the observed T_{dp} agrees very well with those in Ref. 17, when we use the same definitions as in Ref. 17 and the data near the sample edge. T_{dp} may be the temperature associated with the change of magnetization profile from a V-shaped one due to the bulk pinning to a dome-shaped one due to the surface/geometrical pinning, as has been suggested.[17] A change in the profile near 28 K, close to T_{dp}, has indeed been observed from local magnetization,[34] electron spin resonance[35] and the magnetic relaxation.[36] The crossover of the dominant pinning mechanism takes place locally when the magnetization becomes nearly 10 G, where the effect of a bulk pinning on the profile is almost the same as that of the surface/geometrical pinning. It has been suggested[36,37] that around 25 K, the creep mechanism of the vortex-line system is attributable to the collective creep theory,[38] which would explain the increasing activation barrier with decreasing magnetization, i.e., increasing induction B. On the contrary, the surface/geometrical barrier is expected to decrease with increasing induction B.[19,39] The T_{dp} is the temperature where this crossover in the creep mechanisms takes place. The crossover in the creep mechanisms takes place at first at the top of the dome-shaped profile and gradually spreads all over the sample, when B is increased.

If the DL terminates at a critical point, then bulk pinning should vanish at a temperature above the critical point. This is plausible only in the case of the optimally doped sample, since, for the underdoped and the overdoped samples, the bulk pinning seems to persist up to the temperature where the magnetization cusp is observed. For the optimally doped sample, IL in the solid phase (below B_m) may tend to the DL, if the sample has good homogeneity and the geometrical barrier[19] is removed. It is suggested that the IL (both above and below the B_m) agrees with the DL, and connects to the critical point.[17] The continuity and temperature dependence of the boundaries near the critical point resemble a tricritical behavior as observed for the spin system.[40] In fact, the observed critical point is not such a tricritical point, since the IL and DL are not phase boundaries but represent crossover of pinning mechanisms. Details of the magnetic relaxation undertaken to understand the IL and the DL have been partly reported[37] and more details will be published elsewhere.

V. SUMMARY

The vortex-matter phase diagram of underdoped, as-grown (nearly optimally doped) and overdoped Bi2212 crystals has been examined by use of a Hall-sensor array. The first-order ML, which manifests itself as a step in magnetization curves, has been detected at relatively high temperatures for all the samples. The position in the field of the second peak in magnetization at low temperatures has been determined definitively from the relaxed magnetization near the sample edge after a sufficiently long waiting time. At intermediate temperatures, for the underdoped and optimally doped samples, either the second peak or the magnetization cusp that connects to the step, has been observed at the same temperature and the same field but in different experimental time scales. It has been demonstrated that in all the samples the onset field of the second peak, which is interpreted as an EL, connects continuously with the ML. The ML for the three samples corresponds to a single curve when a scaling

of $(T_C^2-T^2)/T_C T\lambda^2\gamma^2$ (λ is the penetration depth and γ the anisotropy constant) is used against the induction B, consistent with the decoupling theory. The EL is well fitted by $B \propto (1+cT^2)/\gamma^2$, with $c>0$, suggesting a presence of dimensional crossover. The positions of the DL and the irreversibility line IL, measured by temperature sweep and field sweep, respectively, are found to depend on the time scale of the sweep rate, suggesting that they represent crossovers between two different vortex-creep mechanisms. Only the ML-EL is proposed to be the real phase boundary. The importance of the spatial profile of the magnetization and its relaxation have been emphasized to clarify these phase boundaries.

ACKNOWLEDGMENTS

We are thankful to T. Tamegai for useful discussions on fabrication of micro-Hall sensors. We would like to thank K. Oka for his help in the crystal growth and T. Yanagisawa for critical reading of the manuscript. One of the authors (G.R.) acknowledges NEDO and ISTEC. Another author (A.M.) thanks JRDC for support.

*Present address: University of Hyderabad, Hyderabad 500 046, India.

†Present address: Quaid-i-Azam University, Islamabad, Pakistan.

[1] G. Blatter, M. V. Feigel'man, V. B. Geshkenbein, A. I. Larkin, and V. A. Vinokur, Rev. Mod. Phys. **66**, 1125 (1994).

[2] H. Pastoriza, M. F. Goffman, A. Arribere, and F. de la Cruz, Phys. Rev. Lett. **72**, 2951 (1994).

[3] Y. Yamaguchi, N. Aoki, F. Iga, and Y. Nishihara, Physica C **246**, 2164 (1995).

[4] E. Zeldov, D. Majer, M. Konczykovski, V. B. Geshkenbein, V. M. Vinokur, and H. Shtrikman, Nature (London) **375**, 373 (1995).

[5] D. T. Fuchs, E. Zeldov, T. Tamegai, S. Ooi, M. Rappaport, and H. Shtrikman, Phys. Rev. Lett. **80**, 4971 (1998).

[6] T. Giamarchi and P. Le Doussal, Phys. Rev. B **55**, 6577 (1997).

[7] D. Ertaz and D. R. Nelson, Physica C **272**, 79 (1996).

[8] V. Vinokur, B. Khaykovich, E. Zeldov, M. Konczykowski, R. A. Doyle, and P. H. Kes, Physica C **295**, 209 (1998).

[9] M. F. Goffman, J. A. Herbsommer, F. de la Cruz, T. W. Li, and P. H. Kes, Phys. Rev. B **57**, 3663 (1998).

[10] R. Cubitt, E. M. Forgan, G. Yang, S. L. Lee, D. McK. Paul, H. A. Mook, M. Yethiraj, P. H. Kes, T. W. Li, A. A. Menovsky, Z. Taenawski, and K. Mortensen, Nature (London) **365**, 407 (1993).

[11] A. Oral, J. C. Barnard, S. J. Beending, I. I. Kaya, S. Ooi, T. Tamegai, and M. Henini, Phys. Rev. Lett. **80**, 3610 (1998).

[12] T. Tamegai, Y. Iye, I. Oguro, and K. Kishio, Physica C **213**, 33 (1993).

[13] S. Anders, R. Parthasarathy, H. M. Jaeger, P. Guptasarma, D. G. Hinks, and R. van Veen, Phys. Rev. B **58**, 6639 (1998).

[14] B. Khaykovich, E. Zeldov, D. Majer, T. W. Lee, P. H. Kes, and M. Konczykowski, Phys. Rev. Lett. **76**, 2555 (1996).

[15] A. Mumtaz, Y. Yamaguchi, K. Oka, and G. Rajaram, Physica C **302**, 331 (1998).

[16] Y. Yamaguchi, G. Rajaram, N. Shirakawa, H. Obara, T. Nakagawa, A. Mumtaz, and H. Bando, in *Advances in Superconductivity XI, Proceedings of ISS'98*, edited by K. Koshizuka and S. Tajima (Springer-Verlag, Tokyo, 1999), p. 223.

[17] C. D. Dewhurst and R. A. Doyle, Phys. Rev. B **56**, 10 832 (1997).

[18] S. Ooi, T. Shibauchi, and T. Tamegai, Physica C **302**, 339 (1998).

[19] E. Zeldov, A. I. Larkin, V. B. Geshkenbein, M. Konczykowski, D. Majer, B. Khaykovich, V. M. Vinokur, and H. Shtrikman, Phys. Rev. Lett. **73**, 1428 (1995).

[20] P. H. Kes, H. Pastriza, T. W. Li, R. Cubitt, E. M. Forgan, S. L. Lee, M. Konczykowski, B. Khaykovich, D. Majer, D. T. Fuchs, and E. Zeldov, J. Phys. I **6**, 2327 (1996).

[21] L. I. Glazman and A. E. Koshelev, Phys. Rev. B **43**, 2835 (1991).

[22] L. L. Daemen, L. N. Bulaevskii, M. P. Maley, and J. Y. Coulter, Phys. Rev. B **47**, 11 291 (1993); Phys. Rev. Lett. **70**, 1167 (1993).

[23] G. Blatter, V. Geshkenbein, A. Larkin, and H. Nordberg, Phys. Rev. B **54**, 72 (1996).

[24] T. Jacobs, S. Sridhar, Qiang Li, G. D. Gu, and N. Koshizuka, Phys. Rev. Lett. **75**, 4516 (1995).

[25] J. C. Martinez, S. H. Brongersma, A. Koshelev, B. Ivlev, P. H. Kes, R. P. Gressen, D. G. de Groot, Z. Tarnavski, and A. A. Menovsky, Phys. Rev. Lett. **69**, 2276 (1992).

[26] Y. Watanabe, T. Fujii, and A. Matsuda, Phys. Rev. Lett. **79**, 2113 (1997).

[27] T. W. Li, A. A. Menovsky, J. J. M. Franse, and P. H. Kes, Physica C **257**, 179 (1996).

[28] O. Waldmann, F. Steimeyer, P. Muller, J. J. Neumeier, F. X. Regi, H. Savary, and J. Scneck, Phys. Rev. B **53**, 11 825 (1996).

[29] Y. Ando, S. Komiya, Y. Kotaka, and K. Kishio, Phys. Rev. B **52**, 3765 (1995).

[30] R. A. Doyle, D. Liney, W. S. Seow, A. M. Campbell, and K. Kadowaki, Phys. Rev. Lett. **75**, 4520 (1995).

[31] T. Shibauchi, T. Nakao, M. Sato, T. Kisu, N. Maeda, N. Okuda, S. Ooi, and T. Tamegai, Phys. Rev. Lett. **83**, 1010 (1999).

[32] V. M. Vinokur, B. H. Kes, and A. E. Koshelev, Physica C **168**, 29 (1990).

[33] H. Pastriza, F. de la Cruz, D. B. Mitzi, and A. Kapitulnik, Phys. Rev. B **46**, 9278 (1992).

[34] E. Zeldov, D. Majer, M. Konczykowski, A. I. Larkin, V. M. Vinokur, V. B. Geshkenbein, N. Chikumoto, and H. Shtrikman, Europhys. Lett. **30**, 367 (1995).

[35] R. I. Khasanov, Yu. I. Talanov, W. Assmus, and G. B. Teite'baum, Phys. Rev. B **54**, 13 339 (1996).

[36] M. Niderost, A. Suter, P. Visani, A. C. Mota, and G. Blatter, Phys. Rev. B **53**, 9286 (1996).

[37] Y. Yamaguchi, G. Rajaram, N. Shirakawa, A. Mumtaz, H. Obara, T. Nakagawa, and H. Bando, in *Advances in Superconductivity XII, Proceedings of ISS'99*, edited by T. Yamashita and K. Tanabe (Springer-Verlag, Tokyo, 2000), p. 326.

[38] M. V. Feigel'man, V. B. Geshkenbein, A. I. Larkin, and V. A. Vinokur, Phys. Rev. Lett. **63**, 2303 (1989).

[39] A. E. Koshelev, Physica C **223**, 276 (1994).

[40] L. J. deJongh and A. R. Miedema, *Experiments on Simple Magnetic Model Systems* (Taylor & Francis, London, 1974), p. 222.